Peptide-Guided Organization of Peptide−Polymer Conjugates: Expanding the Approach from Oligo- to Polymers

Jens Hentschel, Mattijs G. J. ten Cate, and Hans G. Börner*

Max Planck Institute of Colloids and Interfaces, MPI KG Golm, 14424 Potsdam, Germany

Received August 10, 2007; Revised Manuscript Received September 20, 2007

ABSTRACT: The synthesis and self-assembly behavior of a set of peptide−polymer conjugates is described. It is demonstrated that an oligopeptide segment, composing 3.5 wt % of a conjugate, can effectively direct the microstructure formation of a poly(*n*-butyl acrylate)-block (p*n*BA) with $M_n \approx 38\,000$. RAFT polymerization is used to synthesize conjugates possessing p*n*BA blocks with different block lengths ($M_n = 8000-38\,000$) but having the same peptide−aggregator domain. The high tendency of this peptide to adopt a β-sheet is temporarily suppressed by switch and pseudoproline defects, allowing the ease of introduction of a RAFT chain-transfer moiety (CTA). The resulting peptide-CTA can effectively mediate the polymerization of *n*-butyl acrylate, leading to a conjugate with suppressed aggregation tendency. However, the undisturbed peptide segment is reestablished via a pH-controlled rearrangement in the defects, triggering peptide-directed microstructure formation. Atomic force microscopy (AFM) allows the visualization of fibrillar microstructures and frequently provides evidence for a left-handed superhelical fine structure. The peptide segments organize into β-sheets as proven by infrared spectroscopy (FT-IR) and electron diffraction coupled to transmission electron microscopy (SAED-TEM). Thus, peptide organization controls microstructure formation and both the dimensions of the fibrils and the approximated rates of self-assembly are correlated to the molecular weight of the p*n*BA blocks in the conjugates.

Introduction

Biomacromolecules such as nucleic acids, proteins, and increasingly polysaccharides are recognized to fulfill broad spectra of tasks within biological systems.[1−4] To realize frequently very complex functions, the ability to self-organize into functional structures with a remarkable chemical diversity is mandatory.[5] Therefore, these classes of bioorganic polymers inspired the design of synthetic polymer materials having, on one hand, the potential to expand the structural and functional space available for "common" polymers, like, for instance, that of AB-block copolymers.[6−14] On the other hand, material interfaces might be realizable, enabling one to actively interact with biological systems and potentially control biosystems.[15−18]

Nature offers many biomaterials that possess excellent properties, including strength, toughness, elasticity, and lightweight construction (e.g., silks,[19] protein glues,[20] seashells,[21] bones,[22] connective proteins in muscles[23]). Frequently the mechanical properties are beyond those of synthetic polymers.[24] As a consequence academic and applied industrial interests for polymer materials, designed to mimic advanced properties of biomaterials, have increased enormously within the last years.[25]

Recently peptide-guided organization of synthetic polymers proved to be a versatile tool to obtain bioinspired materials with advanced structural control.[26] Synthetic polymers were conjugated to sequence-controlled peptide segments. The latter exhibited high propensities to self-assemble either spontaneously or in a triggered manner into strongly anisometric micro- or nanostructures.[27−30] In these approaches formation of the β-sheet secondary structure motif is essential for self-assembly into tapes, filaments, or fibers.[31] However, despite all advances in structural control, industrial applicability is clearly limited by both the high production costs of well-defined peptides and the efforts necessary to integrate these into synthetic polymers. As a direct consequence it is essential to minimize the fraction of the required 'biosegments' in the polymer−peptide block copolymers (polymer−peptide conjugates), while maintaining the functions of these bioinspired polymers.

As this is an important requirement for large-scale industrial applicability of peptide−polymer conjugates, possible synthesis routes have to be considered carefully.[32] There are two main approaches to integrate sequence-controlled peptides into synthetic polymers: (i) direct coupling of peptides to synthetic polymers and (ii) grafting of polymers from a peptidic macroinitiator. The direct coupling approach relies on the coupling of a selectively addressable functionality that is present in an oligopeptide with a complementary end group of a synthetic polymer.[33−35] The strategy, however, is strongly limited to polymers with fairly low molecular weights due to a decrease in chain end group reactivity with increasing molecular weight.[36,37]

This obstacle can be avoided by following a polymerization strategy that allows access to well-defined polymer−bioconjugates with high molecular weight polymer blocks. Controlled radical polymerization techniques (CRP[38]) have shown to be most suitable. It was demonstrated that sequence-defined polypeptides can be selectively functionalized and applied as macroinitiators for nitroxide-mediated radical polymerization (NMP)[39] and atom transfer radical polymerization (ATRP).[40−42] Moreover, introduction of a chain-transfer moiety to an oligopeptide allows the effective mediation of a reversible addition−fragmentation chain-transfer radical polymerization (RAFT).[43] In particular, the tolerance against many functional groups, absence of metal catalysts, and close relation of the RAFT process to conventional free-radical polymerizations are advantages for the synthesis of bioconjugates. Peptide-based chain-transfer agents (peptide-CTAs) were obtained by the clean transformation of an ATRP initiator group of a solid-phase-supported oligopeptide ATRP macroinitiator into a chain-transfer moiety. After liberating the peptide-CTA from the support, polymerization of *n*-butyl acrylate (*n*BA) was effectively mediated in solution, resulting in conjugates with controllable

* To whom correspondence should be addressed. Phone: +49-(0)331-567-9552. Fax: +49-(0)331-567-9502. E-mail: hans.boerner@mpikg.mpg.de.

10.1021/ma071810z CCC: $37.00
Published on Web 11/29/2007

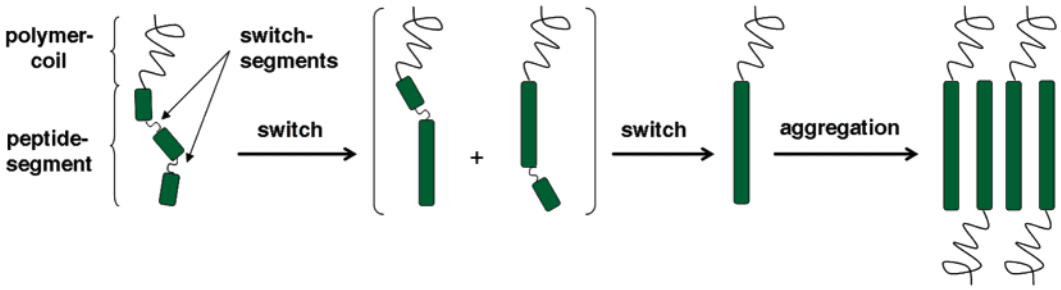

Figure 1. pH-controlled switch of a polymer−peptide conjugate with two switch defects in the peptide segment (two-step process from the fully disturbed peptide segment (left) via two intermediate structures (middle) to the undisturbed aggregator (right).

molecular weights and low polydispersities of $M_w/M_n \approx 1.1$.[43]

In both the direct coupling strategy and the polymerization approach difficulties can occur due to aggregation of the peptide segments during synthesis, analysis, and polymer conjugation. Synthesis of β-sheet-forming peptides, for instance, is often highly ineffective because microaggregation of the peptide segments can take place on the solid support.

Recently, synthesis of peptides, exhibiting highly difficult sequences such as the amyloid Aβ_{1-42} or the (threonine−valine)-multimer aggregator domain, e.g., $(Thr\text{-}Val)_5$, was facilitated by introduction of temporary structure breaking defects. These defect segments are referred to as "switch" segments,[44−46] and previously incorporation of multiple "switch" segments in a $(Thr-Val)_5$ oligopeptide was reported.[30,47] The defects exhibit a β-ester connectivity between Val^n and Thr^{n+1} instead of the native α-amide linkage (cf. Scheme 1). This disturbs the peptide function and suppresses the aggregation tendency. However, after successful synthesis of the peptide−polymer conjugate a pH-controlled rearrangement could be triggered in the switch segments, restoring the native peptide backbone and thus allowing for a controlled activation of the aggregation tendency. It was demonstrated that the switch segments are potent tools for the peptide-guided microstructure formation of synthetic polymers because aggregation kinetics can be controlled (cf. Figure 1).[30,48] However, the concept was only demonstrated with low molecular weight polymers (M_n= 2000−3000).

Here we present the synthesis and self-assembly behavior of peptide−polymer conjugates, exhibiting high molecular weight polymer blocks and a switchable β-sheet-forming oligopeptide as an aggregator domain. The RAFT polymerization approach was applied, utilizing a peptide-CTA with temporarily disturbed aggregation tendency (switch peptide as macrotransfer agent). The peptide-directed microstructure formation of the resulting conjugates was studied intensively and correlated to the molecular weight of the synthetic polymer blocks.

Experimental Section

The materials and instrumentation as well as the synthetic procedure for the switch-peptide precursor (**I**) and switch-peptide chain-transfer agent (**II, III**) are provided in the Supporting Information.

The idealized models of the superhelical aggregates (Figure 4) are not the result of computer simulation. However, the position of the peptide segments as graphical objects was calculated, resulting in object translation and rotation that takes the β-sheet distortion angles γ_θ (twist) and γ_ν (bend) into account.

Synthesis of Conjugates (Ph−C(S)-S-(p*n*BA)$_n$-CH(CH$_3$)-C(O)-Thr(tBu)-(Val-Thr)^{pro}-Val-Thr(tBu)-(Val-Thr)^{switch}-(Val-Thr)^{pro}-Val-Gly-NHCH$_2$CH$_2$OH) (IV). *General Procedure.* The switch-peptide transfer agent **III** (20 mg, 12.3 μmol) was dissolved in DMF (4.0 mL) and stirred overnight under an argon atmosphere. A 0.5 mL of a stock solution of AIBN in DMF (0.40 mg·mL^{-1}, 1.2 μmol) was added followed by *n*BA (0.5 mL, 3.49 mmol). The reaction mixture was carefully degassed with argon and heated to 60 °C. Samples were taken for kinetic analysis (GPC, NMR). Depending on the desired molecular mass the polymerization was stopped by rapid cooling to room temperature and exposure of the reaction mixture to air. The sample was concentrated in vacuo; then it was precipitated multiple times from MeOH in ice−water and freeze-dried from acetonitrile/benzene (1:1) to extract eventually remaining peptide or peptide transfer agent. Three different p*n*BA conjugates (**IV-8k**, **IV-14k**, **IV-38**) were synthesized, utilizing this polymerization procedure. The resulting conjugates were characterized using GPC and NMR spectroscopy.

IV-8k. ^{1}H NMR (DMSO-d_6 (2.49 and 3.31 ppm)): δ = 0.78−1.76 (m, 669 H, 30 H C(C*H*$_3$)$_2$ Val + 195 H CH$_2$−C*H*$_3$ + 12 H C(C*H*$_3$)OH Thr + 3 H C(C*H*$_3$)O−CO Thr + 3 H S−C(C*H*$_3$)−CO + 18 H C(C*H*$_3$)$_3$ ^{t}Bu + 12 H C(C*H*$_3$)$_2$ PP + 9 H C(C*H*$_3$)$_3$ Boc + 130 H C*H*$_2$−CH$_3$ p*n*BA + 130 H CH$_2$−C*H*$_2$−CH$_2$ + 130 H CH−C*H*$_2$ p*n*BA), 1.98−2.31 (m, 70 H, 5 H C*H*(CH$_3$)$_2$ Val + 65 H, C*H*−CH$_2$ p*n*BA), 3.64−4.34 (m, 151 H, 12 H α-C*H* + 4 H C*H*−OH Thr + 4 H HO−C*H*$_2$−C*H*$_2$ + 1 H S−C*H*(CH$_3$)−CO + 130 H O−C*H*$_2$ p*n*BA), 5.26 (t, 1 H, C*H*−O−CO Thr), 7.29−8.51 (m, 15 H, 5 H ArH + 10 H N*H*) ppm. $M_{n,conj.}$ = 9900, DP$_n$ = 65. GPC (THF, p*n*BA-standards): $M_{n,app}$ = 11 000, DP$_n$ = 69, M_w/M_n = 1.29.

IV-14k. ^{1}H NMR (DMSO-d_6): $M_{n,conj.}$ = 15 800, DP$_n$ = 111, determined by comparison of the characteristic ^{1}H NMR resonances resulting from p*n*BA at 4.05−4.10 ppm (OC*H*$_2$) with these of the oligopeptide segment (δ = 5.26 ppm (C*H*−O−CO Thr$_{ester}$)) and the CTA group (δ = 7.40−7.47 ppm (ArH$_{meta}$)). GPC (THF, p*n*BA standards): $M_{n,app}$ = 16 000, DP$_n$ = 110, M_w/M_n = 1.25.

IV-38k. ^{1}H NMR (CDCl$_3$): $M_{n,conj.}$ = 39 000, DP$_n$ = 292, determined by comparison of the characteristic ^{1}H NMR resonances resulting from p*n*BA at 4.05−4.10 ppm (OC*H*$_2$) with those of the CTA group (δ = 7.34−7.96 ppm (ArH)). GPC (THF, pS standards): $M_{n,app}$ = 37 000, DP$_n$ = 274, M_w/M_n = 1.33.

Deprotection of the Conjugates. To cleave the protecting groups, the conjugates were dissolved in a mixture of 30% TFA in DCM and the solution was gently shaken for 30 min. Afterward dioxane was added, and the organic solvents were removed in vacuo at room temperature. The resulting product was lyophilized from acetonitrile/benzene (1:1).

IV-8k. ^{1}H NMR (MeOH-d_4 (3.30 and 4.84 ppm)): δ 0.80−1.10 (m, 225 H, 30 H C(C*H*$_3$)$_2$ Val + 195 H CH$_2$−C*H*$_3$), 1.16−1.95 (m, 408 H, 12 H C(C*H*$_3$)OH Thr + 3 H C(C*H*$_3$)O−CO Thr + 3 H S−C(C*H*$_3$)−CO + 130 H C*H*$_2$−CH$_3$ p*n*BA + 130 H CH$_2$−C*H*$_2$−CH$_2$ + 130 H CH−C*H*$_2$ p*n*BA), 2.10−2.42 (m, 70 H, 5 H C*H*(CH$_3$)$_2$ Val + 65 H C*H*−CH$_2$ p*n*BA), 3.64−4.34 (m, 151 H, 12 H α-C*H* + 4 H C*H*−OH Thr + 4 H HO−C*H*$_2$−C*H*$_2$ + 1 H S−C*H*(CH$_3$)−CO + 130 H O−C*H*$_2$ p*n*BA), 5.28 (t, 1 H, C*H*−O−CO Thr), 7.45−7.97 (m, 5 H ArH) ppm. $M_{n,conj.}$ = 9700, DP$_n$ = 66.

IV-14k. ^{1}H NMR (DMSO-d_6): $M_{n,conj.}$ = 16 700, DP$_n$ = 120, determined by comparison of the characteristic ^{1}H NMR resonances resulting from p*n*BA at 4.05−4.10 ppm (OC*H*$_2$) with these of the CTA group (δ = 7.49−7.51 ppm (ArH$_{meta}$)).

IV-38k. ^{1}H NMR (CDCl$_3$): $M_{n,conj.}$ = 38 000, DP$_n$ = 285 determined by comparison of the characteristic ^{1}H NMR resonances

Scheme 1. Synthesis of the Oligopeptide CTA (III)[a]

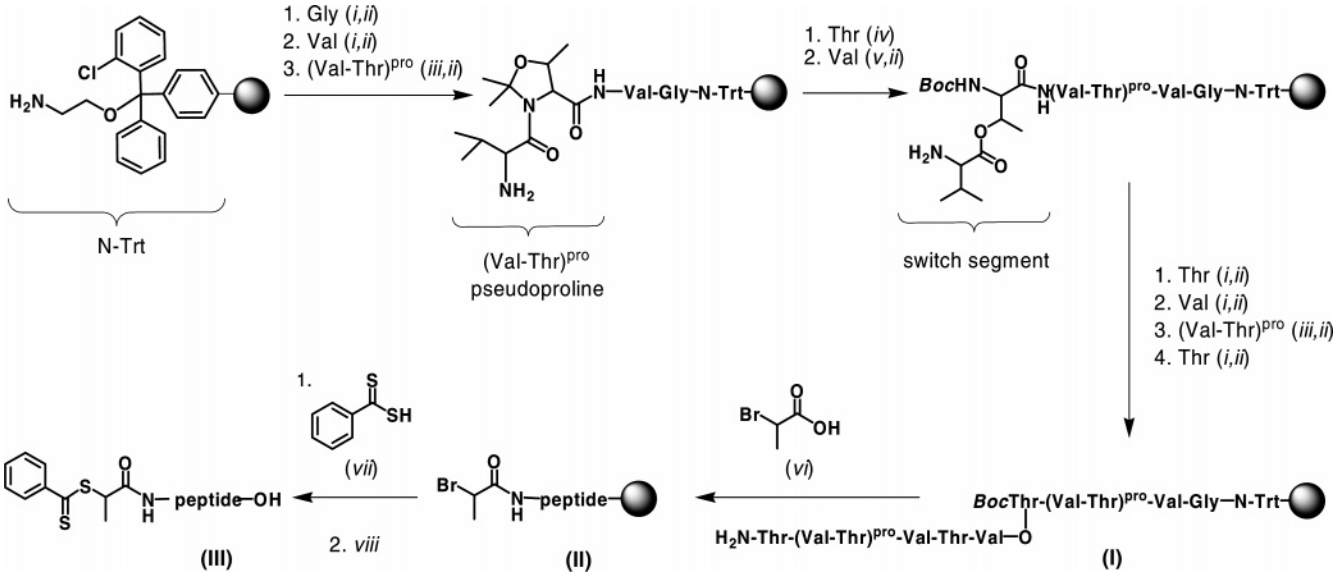

[a] Reagents and conditions: 2-aminoethanol-2-chloro-trityl-polystyrene resin; (i) Fmoc-Aa, HBTU/DIPEA/NMP, 20 min.; (ii) 20 vol % piperidine/NMP; (iii) Fmoc-Val-Thr($\Psi^{Me,Me}$pro) OH, PyBOP/HOBt/DIPEA/DMF, 2 × 1 h; (iv) Boc-Thr OH, HBTU/DIPEA/NMP, 20 min; (v) Fmoc-Val OH, DIC/NMI/DCM, 2 × 2 h; (vi) DCC/DIPEA/DMF; (vii) pyridine, THF, 60 °C, 2 × 20 h; (viii) 2 vol % TFA in DCM (3 × 1 min).

resulting from p*n*BA at 4.00−4.06 ppm (OCH_2) with these of the CTA group (δ = 7.35−7.96 ppm (ArH)).

Switch and Self-Assembly Procedure. For a typical sample 1 mg of the conjugate (**IV**) was dissolved in 1 mL of a mixture of diethyl ether and MeOH (70:30). To prevent early, uncontrolled switching the solution was immediately stabilized with 20 mg of TFA. To ensure reproducibility of the conditions during the switch the "amount of acid" present in the Et_2O/MeOH solution (apparent pH value) was estimated by diluting 10 μL of the solution with 3 μL of deionized water and measuring the pH with a standard indicator paper (range of pH indicator 2−5 and 5−8). Prior to the aggregation process the switch in the peptide segment was induced by titration of the TFA 0.1 M methanolic NaOH (70:30)). The apparent pH of the solution of **IV** was adjusted to $pH_{app.}$ = 6.0, allowing the slow transition to **V**. During the switch and subsequent aggregation the solution was gently shaken at room temperature.

Results and Discussion

To extend the strategy of peptide-guided microstructure formation of organo-soluble, peptide−polymer conjugates from conjugates with low molecular weight synthetic polymers ($M_n \approx 2000-3000$) toward high molecular weight systems a peptide-CTA was synthesized and utilized for the RAFT polymerization of *n*-butyl acrylate (*n*BA). Poly(*n*-butyl acrylate) (p*n*BA) was chosen because of interesting adhesion properties, a low T_g, and the absence of crystallinity. Thus, interference of the peptide organization process with, e.g., polymer crystallization or glass formation is not expected. Combination of the RAFT "grafting from" strategy with peptide organizer segments, however, might allow for incorporation of diverse polymer blocks. Self-assembly of the conjugates is dominated by the directed interactions between the peptide segments and takes place in dilute solution, where the polymer block is well solvated. Therefore, a variety of polymers could potentially be organized in complex structures, providing microstructures with different functionalities and functions.

To effectively direct and control the microstructure formation in peptide−polymer conjugates, a peptide segment with the amino acid sequence (Thr−Val)$_5$-Gly (Scheme 1, **I**), where Val = valine, Thr = threonine, and Gly = glycine, was utilized. Such domains, consisting of repeats of alternating threonines and valines ((TV)$_5$), are known to exhibit a high propensity to adopt a stable β-sheet in water[30,49,50] as well as in some organic solvents.[48] The (TV)$_5$ aggregator domain was capped on the C-terminal side with a Gly, increasing the solubility and reducing entropic penalties during β-sheet formation. As mentioned before, strongly aggregating peptides are difficult to synthesize via solid-phase-supported peptide synthesis (SPPS).[51] In the continuing efforts to extend the SPPS to a generic platform that allows the synthesis of peptides, independent of their monomer sequence, multiple strategies were developed to overcome the problem of "difficult sequences". Beside others, incorporation of temporary structure breaking defects, like, for instance, the switch segment[44−46] and the pseudoproline unit,[52] is a powerful tool to facilitate peptide synthesis. Recently incorporation of two or four switch segments into a (TV)$_5$ domain was reported, and the excellent potential of these defects to suppress the aggregation tendency was demonstrated.[30,48] Even if the introduction of multiple switch segments in a peptide aggregator domain effectively ensures suppression of the aggregation tendency, a high number of possible intermediates make the switch process complex. As schematically illustrated in Figure 1 incorporation of two switch segments into a (TV)$_5$ domain results in two different intermediates, and in the case of four switch defects 14 intermediates could be formed. Because the aggregation tendency of a peptide segment in a conjugate is gradually increasing with the length of the continuous, nondisturbed (TV)$_x$ domain, a highly predictable switching process requires minimization of the possible intermediates. Therefore, the number of switch defect segments was reduced to one, allowing for establishment of a binary OFF and ON stage.

However, use of only one defect in a (TV)$_5$ domain between Val^6 and Thr^7 increases the difficulties during synthesis because two native (Val−Thr)$_2$ segments already exhibit a weak aggregation tendency. Hence, two pseudoproline units were incorporated between Val^2−Thr^3 and Val^8−Thr^9, inhibiting aggregation of the peptide segment during SPPS. Scheme 1 illustrates the synthesis of the peptide-CTA (**III**), exhibiting temporarily disturbed aggregation tendency by both switch and pseudoproline segments.

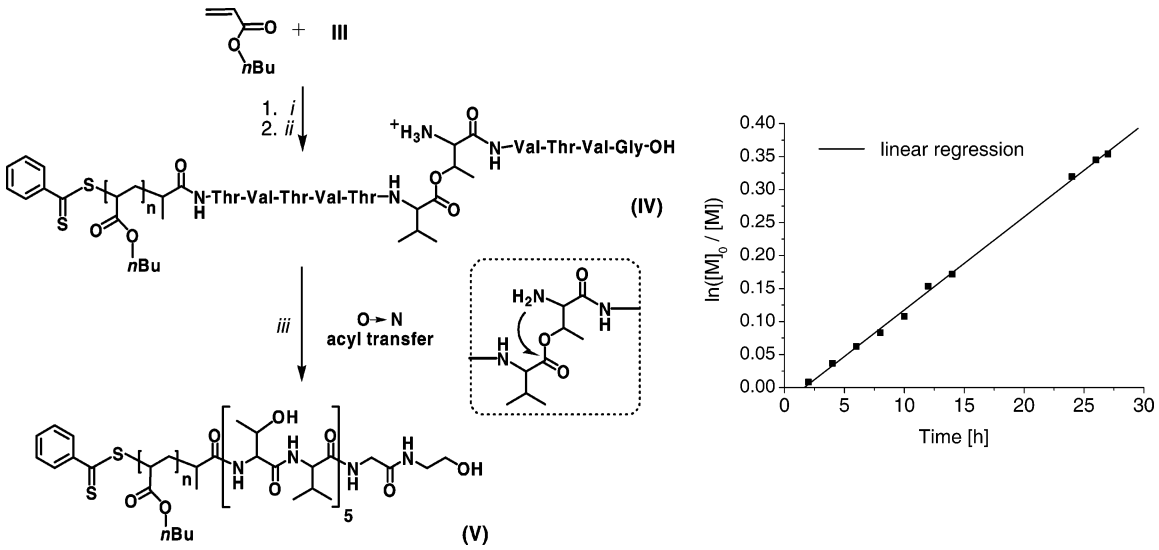

Figure 2. (left) Synthesis of the p*n*BA−peptide conjugates (**IV**) via RAFT polymerization and switching into the native, all-amide species (**V**) (reagents and conditions: (i) *n*Bu, AIBN, DMF, 60 °C; (ii) 30 vol % TFA/DCM; (iii) adjustment of the apparent pH of a dilute solution of **IV** in Et_2O/MeOH to ∼6.0), and (right) semilogarithmic plot of the RAFT radical polymerization of *n*BA, mediated by **III (**monomer conversion vs reaction time; $[n\text{BA}]_0/[\textbf{III}]_0/[\text{AIBN}]_0 = 285/1/0.1$, DMF = 90 vol %).

The peptide segment **I** was obtained in a semi-automated SPPS procedure by the sequential assembly of standard Fmoc amino acid derivatives and the pseudoproline units. The latter are Fmoc-protected dipeptides (Fmoc−Val−Thr($\Psi^{\text{Me,Me}}$pro)OH), which were coupled via bench top techniques. Incorporation of the switch ester segment, positioned in the middle of the peptide sequence between Val[6] and Thr[7], proceeded in a smooth manner using bench top coupling.[48] After completion of **I** the chemical structure was verified by electrospray mass spectrometry (ESI-MS) and ^{1}H NMR techniques. A small fraction was cleaved from the support, while removing all protecting groups from the peptide segment. ESI-MS measurements confirmed the successful synthesis of **I** by showing the appropriate mass signal at *m*/*z* 1119.2, assignable to $[M_{\textbf{I}} + H]^+$ (cf. Supporting Information Figure S1). This was verified by ^{1}H NMR, showing the presence of one switch threonine ester ($\delta = 1.33-1.35$ ppm; C(C*H*$_3$)O−CO) and four native threonine amides ($\delta = 1.13-1.29$ ppm; C(C*H*$_3$)OH) with respect to the resonances of five valine residues ($\delta = 2.07-2.21$ ppm; C*H*(CH$_3$)$_2$).

The RAFT initiator moiety was introduced at the N-terminal side of the supported peptide **I** utilizing a two-step synthesis procedure (Scheme 1).[43] In the first step 2-bromopropionic acid was coupled to the amine group of the resin-bound peptide **I** to give an oligopeptide ATRP initiator (**II**). Quantitative coupling was confirmed by mass spectrometry using a small sample of the fully deprotected **II**, which was cleaved from the support for analysis purposes. ESI-MS shows the corresponding ion adducts $[M_{\textbf{II}} + H]^+$ and $[M_{\textbf{II}} + Na]^+$ and provides no evidence of the nonfunctionalized precursor **I**. The subsequent reaction of the α-bromine group of **II** with dithiobenzoate yields the peptide-CTA (**III**). **III** was isolated as a fully protected peptide after cleavage from the support. ^{1}H NMR verified the chemical identity of **III**. Quantitative conversion was confirmed by comparing the integral intensities of both the five valine residues ($\delta = 2.07-2.18$ ppm; C*H*(CH$_3$)$_2$) and the one switch ester defect ($\delta = 5.26$ ppm; C*H*−O−CO switch Thr) to that of the aromatic dithioester group ($\delta = 7.42-7.96$ ppm; ArH). The clean synthesis of **III** demonstrates that the method of solid-phase supported synthesis of peptide-CTAs can be expanded from model peptides to complex peptide sequences, including systems with temporary switch ester defects.

Table 1. Characterization of the Fully Protected Conjugates

conjugate	$M_{\text{n,pnBA}}$ (NMR)	$M_{\text{n,conj}}$[a]	wt % of p*n*BA[b]	$M_{\text{n,app}}$ (GPC)[c]	M_w/M_n (GPC)[c]
IV[d]**-2k**[e]	2000	3300	60.5	2300	1.13
IV[d]**-8k**	8300	9900	86.5	11 000	1.29
IV[d]**-14k**	14 200	15 800	91.5	16 000	1.25
IV[d]**-38k**	38 000	39 600	96.5	37 000	1.33

[a] $M_{\text{n,conjugate}} \approx (M_{\text{n,pnBA}} + M_{\text{III}})$. [b] Amount of synthetic polymer in the fully deprotected conjugate. [c] Calibrated against pS standards. [d] Protected peptide segment. [e] Synthesized via coupling approach.[48]

As outlined in Figure 2 (left) a series of peptide−polymer conjugates was synthesized using RAFT polymerization of *n*BA mediated by **III**. Polymerization was accomplished in DMF at 60 °C in the presence of **III** as a chain-transfer agent, and AIBN was used to generate the primary radicals. The reaction was followed by GPC and ^{1}H NMR spectroscopy. Figure 2 (right) shows the linear correlation of the monomer conversion with respect to the polymerization time and indicates first-order kinetics after a short retardation period of 1−2 h. Moreover, the molecular weight increases linearly with monomer conversion and M_w/M_n remained nearly constant around 1.2−1.3 (cf. Figure S2). This suggests that RAFT polymerization was effectively mediated by **III** and highlights the tolerance of the RAFT process against rather complex, multifunctional peptide structures.

To correlate the block length of the p*n*BA block with the self-organization behavior of the peptide−polymer conjugates, a set of three different conjugates was synthesized, which exhibit the same aggregator domain but differ in the lengths of the p*n*BA blocks. The resulting peptide−polymer conjugates were isolated after careful precipitation and lyophilization from acetonitrile/benzene. Analysis was performed prior to removal of the protecting groups from the peptide segment to avoid difficulties that might result, e.g., from peptide aggregation. GPC revealed the apparent number-average molecular weights ($M_{\text{n,app}}$) and apparent polydispersity indices (M_w/M_n). However, the absolute values for M_n were calculated based on ^{1}H NMR by comparing the integral intensities of the characteristic resonances of the

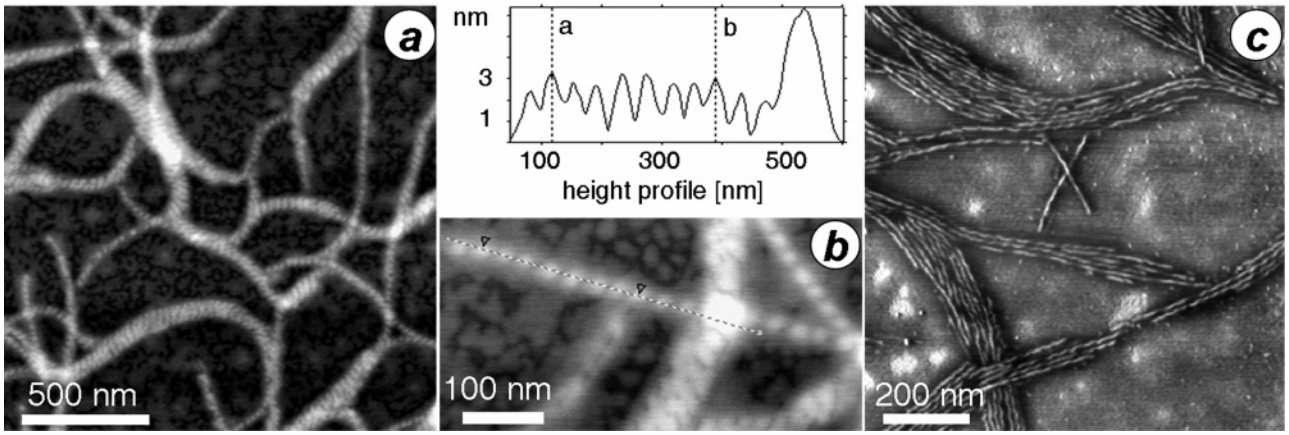

Figure 3. AFM micrograph of the fibrils and fibrillar network formed by the peptide-guided organization of **IV-8k** in solution 12 days after titration (1 mg/mL in Et_2O/MeOH (70%) at $pH_{app} = 6.0$, height image $z = 12$ nm) (a); AFM image of individual fibers with left-handed helical superstructure as well as the corresponding height profile of a single fiber (height image, $z = 12$ nm, low damping) (b); and AFM micrograph showing the packing of individual fibers in the fiber bundles (phase, $z = 70°$, high damping) (c).

p*n*BA block ($\delta = 4.05-4.10$ ppm (O−CH_2)) with these of the oligopeptide segment ($\delta = 5.26$ ppm (CH−O−CO Thr_{ester})) and CTA group ($\delta = 7.34-7.96$ ppm (ArH)). As summarized in Table 1 the conjugates possess $M_{n,conj.}$ between 9900 and 39 000 as well as rather low polydispersity indices. It should be noted that both methods, GPC and NMR, exhibit opposing reliabilities with increasing molecular weight of the conjugate. While the error of $M_{n,NMR}$ progressively increases on molecular weight of the p*n*BA block, the results based on GPC get gradually more accurate due to the decreasing influence of the multifunctional peptide segment on the properties of the conjugate.

After isolation and characterization of the conjugates, all side-chain protecting groups, including the pseudoproline defects, were removed from the peptide segments in order to transform the peptides into switchable aggregator domains (Figure 2, **IV**). This was accomplished by treatment with dilute TFA in DCM followed by lyophilization from acetonitrile/benzene. The cleavage conditions were not affecting the p*n*BA block. This was confirmed by ^{1}H NMR spectroscopy and is consistent with previous observations.[41]

Microstructure Formation of the Polymer−Peptide Conjugates. In analogy to the conjugate p*n*BA_{15}-*block*-$(TV)_5$ (**IV-2k**) that was investigated previously[48] all conjugates prepared via the RAFT route were readily soluble in a mixture of diethyl ether and methanol. However, due to the longer p*n*BA chains the percentage of methanol had to be increased from 10 to 30 vol % to be able to dissolve the conjugates homogeneously. The early O→N acyl transfer rearrangement could be prevented effectively by addition of a small amount of TFA as a stabilizer. This was demonstrated with **IV-8k**. Atomic force microscopy (AFM) provides under these conditions no evidence of microstructure formation in solution after 15 days (cf. Figure S3). Moreover, the presence of ill-defined amide structures was confirmed by infrared spectroscopy (FT-IR), showing a broad Amid I vibration (cf. Figure S4). This indicates that one switch defect effectively disturbs the neighboring $(TV)_2$ domains in the peptide segment of **IV-8k** and suppresses formation of extended β-sheet secondary structures.

Peptide-guided microstructure formation could however be induced if the TFA stabilizer was titrated with a mixture of diethyl ether and methanolic NaOH (70:30 vol %; 0.1 M NaOH in MeOH). Depending on the adjusted apparent pH the switch-defect segments can rearrange and the resulting O→N acyl transfer converts the conjugate with a disturbed peptide segment into a conjugate with a native peptide segment (cf. Figure 2, **IV** → **V**). The latter can express the peptide function, which has in the case of the $(TV)_5$ domain a high tendency to adopt a stable β-sheet.

The process of peptide-guided microstructure formation of polymers was demonstrated with the peptide−polymer conjugate **IV-8k** that possesses a p*n*BA block of $M_n \approx 8000$. It was previously shown that the O→N acyl transfer rearrangement can be performed in Et_2O/MeOH and occurs in a highly controlled manner at apparent pH values from ∼6.0 to ∼7.5.[30,48] By adjusting the $pH_{app.}$ of a dilute solution of **IV-8k** to 6.0 a very slow generation of **V-8k** and thus a rather controlled self-assembly process is expected. Within 2 days formation of anisotropic, fiber-like structures with lengths up to a micrometer were observed by AFM (data not shown). These structures organize further into bundles and fibrillar networks as visualized by AFM after 12 days (Figures 3a and S5). It is important to note that besides the microstructures also unstructured material could be observed. This might be so for nonswitched conjugates, which probably even enrich on the anionic mica substrate due to their cationic character. Detailed kinetic investigations are currently in progress, using analytical ultracentrifugation to quantify the evolution of the structure formation process.

The dominating primary structure elements were investigated more precisely by AFM. As shown in Figure 3b, a distinct fine structure is apparent, consisting of left-handed helical superstructures. Similar motifs were obtained recently by the controlled self-assembly of the conjugate **V-2k**.[48] The analogy between the microstructures and the self-assembled building blocks allows for the straightforward suggestion of a common assembly model. As outlined in Figure 4, at first a flat core−shell nanotape is formed by self-assembly of the peptide aggregators of the conjugates into an antiparallel β-sheet. This assembly step controls the microstructure formation process, leading to flat core shell tapes with a β-sheet core and a p*n*BA shell (Figure 4a and a′). In agreement with theory, describing extended β-sheet structures, e.g., assembled from 11mer oligopeptides,[31] the β-sheet core is distorted by twist (Figure 4 b,b′) and bend distortions of the β-strands, resulting in a helical superstructure (Figure 4 c−e). The distortions are driven by (i) dipole moment effects, (ii) the anisotropic chemical faces of the antiparallel β-sheet, and (iii) probably the steric repulsion of neighboring p*n*BA coils. Moreover, the process is directed by the chirality of the amino acid building blocks, resulting in left-handed helical structures.[31,48] The proposed model is consistent with FT-IR spectroscopy, verifying the presence of

Table 2. Structural Parameters of Helical Fibers of Oligopeptides and Peptide−Polymer Conjugates

	11mer peptide[31]	V-2k	V-8k	V-14k	V-38k
height (AFM), nm		2.9 ± 0.5	3.0 ± 0.8	3.8 ± 0.8	5.2 ± 1.4
width (AFM), nm		13 ± 1	15 ± 3	17.2 ± 2.5	28 ± 5
width (TEM), nm	∼10	10 ± 1	13 ± 2	15 ± 3	30 ± 5
pitch height (AFM), nm	30 ± 15[a]	37 ± 2	59 ± 5		
pitch angle (AFM), deg		48 ± 3	61 ± 5		
max tape width,[b] nm		13.7 ± 2	25.8 ± 3		
$\gamma_{\nu\ \mathrm{bend}}$, deg	∼3	∼2.3	∼1.2		
$\gamma_{\theta\ \mathrm{twist}}$, deg	∼3	∼1.9	∼2.2		

[a] Determined from TEM micrographs. [b] $w_{max} = h_{pitch} \times \sin \alpha_{pitch}$ (with w_{max} as the maximum tape width in the helical superstructure, where α_{pitch} is the pitch angle and h_{pitch} the pitch height).

a β-sheet ($\upsilon_{\mathrm{amide\ I}} = 1628\ \mathrm{cm}^{-1}$ (cf. Figure S4)). Additionally, the peptide organization motif could be directly correlated to the microscopic structures using selected area electron diffraction (SAED) (cf. Figure S6). The typical *d* spacing of 4.8 Å was observed, which is characteristic for the repeat distance of peptides that adopt β-strands in an extended β-sheet.[1]

Formation of a fiber network appears to proceed in a hierarchical manner by the directed organization of primary fiber elements (superhelices) into bundles (Figure 3a and c). This indicates the presence of soft, lateral interactions between the fibers. As evident in Figure 3c, the superhelices are not entangled; in fact, they run parallel over several micrometers and pack densely into bundles. The occurrence of interference pattern in the AFM image of the bundles (cf. Figure 3a) was observed previously already[48] and suggests a clear axial correlation of the superhelices in the bundles. Such in-register packing of helices requires well-defined axial repeats of periodically modulated properties along the helix axis. Probably this could be periodic stickiness caused by the p*n*BA regions and/or periodic dipole moments, resulting from the peptide β-sheets. It is interesting to note that generation of periodic properties along fibers is a fundamental principle abundant in biology, e.g., in collagen filaments, and that this can be mimicked via self-organization of artificial superhelices with periodically modulated axial properties.

Statistical analysis of the AFM images (Figure 3) and TEM micrograph (Figure S5c) allows for determining the structural parameters of the superhelices. These parameters are summarized in Table 2 and should be compared, on one hand, to superhelices formed by the conjugate **V-2k**[48] and, on the other hand, to helical assemblies of a 11mer oligopeptide without polymer.[31]

A strong structural analogy is evident if the helical structures obtained by the self-assembly of **V-8k** with 86 wt % p*n*BA were compared to those of **V-2k** with 61 wt % p*n*BA. Both superstructures appear to be rather soft as indicated by the cross-sectional aspect ratios of $A_R = 3.4$ and 4.3, respectively ($A_R = \mathrm{width_{TEM}/height_{AFM}}$). Probably deformation is induced by substrate contacts and takes place due to strong interactions of the p*n*BA blocks with the high-energy surface of mica, as observed for other nano-objects previously.[53] Intuitively it appears reasonable that **V-8k** assembles to fibers with increased width and height if compared to the **V-2k** structures (Table 2). The increase, however, is not dramatic. This can be explained by the constraints of the peptide β-sheet tape, which seems to have a dominating effect on determining the structural parameters of the superhelices. However, a helix is most easily deformed in a longitudinal manner, resulting in noticeable differences of the pitch height and pitch angle (cf. Table 2). As expected, the pitch height increases from ∼30 nm of a 11mer oligopeptide without polymer[31] to ∼37 nm of the **V-2k** to ∼59 nm of the **V-8k** structures (cf. Figure 4c−e). This is accompanied by an increase in pitch angle from ∼48° to ∼61° of the **V-2k** and the **V-8k** structures, respectively. If the increase of the helix cross-sections is taken into account, the observations appear to be consistent with a simple packing model of a tape because the spatial demands of the tapes that are formed first and subsequently wind into the superhelices are increasing from the oligopeptide to the **V-2k** and to the **V-8k** system.

The theoretical tape width could be calculated assuming that the peptide adopts a β-strand conformation in an antiparallel β-sheet and the p*n*BA forms a statistical coil. While the 11mer oligopeptide results in a tape with ∼4 nm, **V-2k** forms a tape with ∼7 nm and **V-8k** requires about 10 nm. If these values are compared to the maximum tape widths (Table 2) calculated from the pitch heights and pitch angles of the observed superhelices (cf. Supporting Information eq 3), it becomes evident that steric repulsion between the tapes cannot be considered to regulate the structural dimensions of the helices. This highlights the dominating nature of the β-sheet assembly to control the resulting microstructures.

However, the steric repulsion of densely packed neighboring polymer coils in a β-sheet clearly influences the twist and bend distortions of the tape. Given the structure model that suggests a densely wound, twisted, and bent β-sheet tape, the average bending and twisting angles per peptide β-strand can be calculated as described recently (cf. Figure S10, Supporting Information).[31,48] Table 2 summarizes the distortion angles γ_θ (twist) and γ_ν (bend) estimated from the **V-2k** and **V-8k** superhelices. These values can be compared to symmetrical distortion angles of $\gamma_\theta = \gamma_\nu \approx 3°$ published for a β-sheet assembly of a 11mer oligopeptide in water (for idealized structures see Figure 4c−e).[31] It appears that in organic solvents stiffer β-sheet tapes are formed. This is due to the differences in binding energy contributions of H bonds in organic solvents as compared to water, resulting in stronger binding between the β-strands in the β-sheet. While the increase of the molecular weight of the p*n*BA block from 2k to 8k seems to have a minor effect on the twist distortion (Table 2), the bend angle, however, decreases from approximately 2.3° to 1.2°. As a result of the reduced distortions a superhelix with less curvature and larger diameter is generated. This meets the simple model of a distorted spring, and distortion energy results from an increase in steric pressure between densely packed p*n*BA coils in the β-sheet.

It is an important part of the approach of "peptide-guided organization of synthetic polymers"[26] that the peptide segment of a peptide−polymer conjugate directs and drives the microstructure formation process. However, it is very likely that the statistical coil of the synthetic polymer block influences the assembly step progressively on increasing molecular weight. Addressing this issue it is interesting to investigate the differences in the self-assembly behavior of polymer−peptide conjugates depending on the molecular weight of the p*n*BA block. To self-assemble the conjugates **V-14k** and **V-38k** with p*n*BA

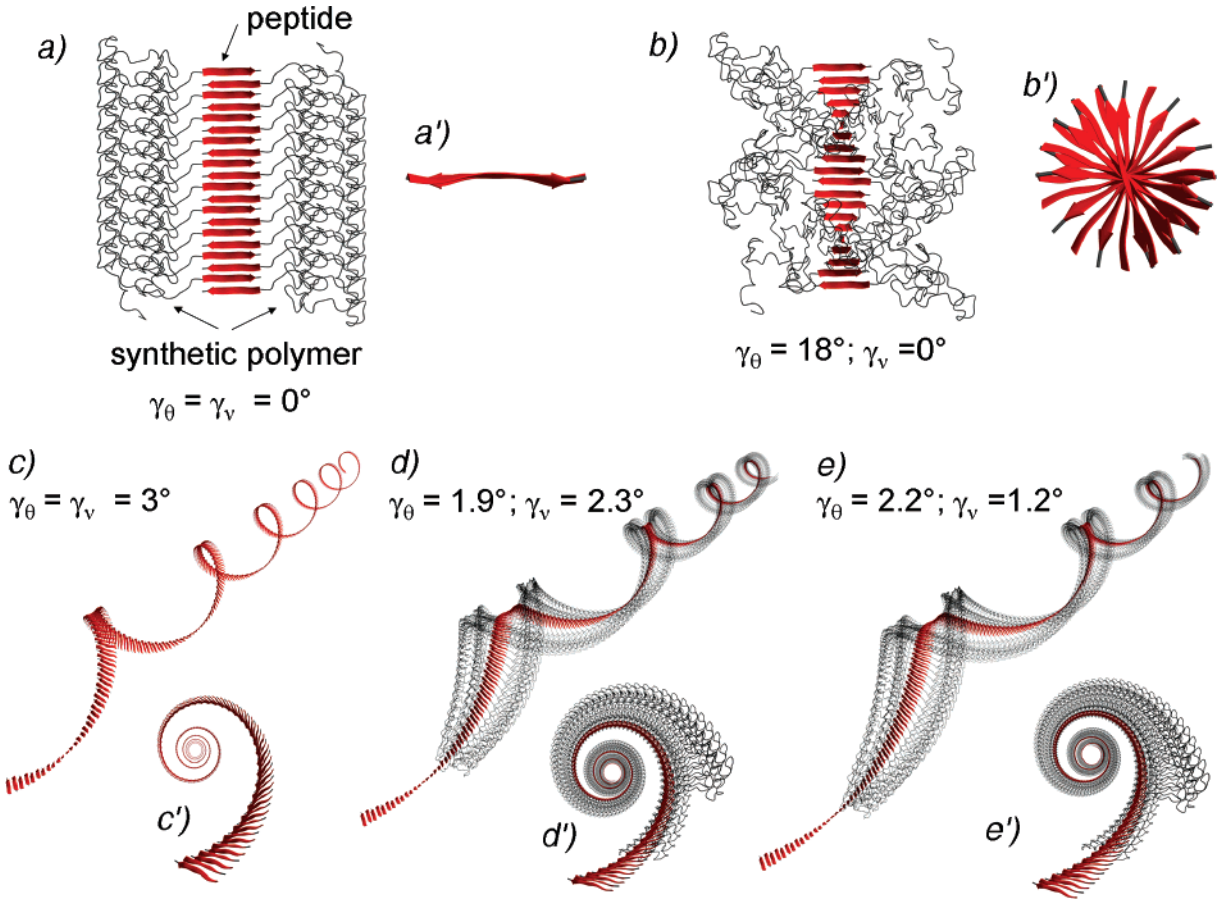

Figure 4. Idealized model of the peptide-guided microstructure formation, where the peptide segments of the peptide−p*n*BA conjugates adopt an antiparallel β-sheet tape that winds into a left-handed helical superstructure (undistorted tape, exhibiting a planar β-sheet and a p*n*BA shell ((a) top view; (a′) front view (polymer coils removed)); core−shell tape with twisted β-sheet core ((b) top view; (b′) front view (polymer coils removed)); β-sheet tape of the 11mer oligopeptide,[31] exhibiting uniform twist and bend distortions ((c) side view, (c′) front view); core−shell tape corresponding to aggregates of **V-2k** with twist and bend distortions ((d) side view, (d′) front view) and distorted core−shell tape of **V-8k** ((e) side view, (e′) front view) ((a−e) positions of the β-sheets were calculated according to specified distortion angles γ_θ and γ_ν; (a, b and d, e) the polymer block and the peptide segment were drawn out of scale due to clarity reasons; (d, e) from the first 20 conjugates the polymer coils were removed).

blocks of $M_n \approx 14\,000$ and 38 000, respectively, similar protocols were followed as described above. The switching process was induced by adjusting the apparent pH of dilute solutions of **IV-14k** and **IV-38k** to about 6.0. Therefore, the O→N acyl switch and generation of the active aggregators **V-14k** and **V-38k** should probably proceed with rates comparable to the **V-8k** system. While the microstructure formation of **V-14k** appears to evolve similarly to **V-8k**, the high molecular weight analogue **V-38k** was found to self-organize considerably slower.

The **V-14k** system allows the visualization of fiber-like structures with AFM after 2 days (data not shown). Even if microstructures are apparent, a high amount of nonstructured material indicates incomplete assembly at this stage. After 16 days, however, distinct fibrillar structures could be observed as shown in Figure 5a. In contrast to this rapid self-assembly, the **V-38k** system organizes significantly slower. After ~50 days at room temperature some indications of fiber formation are evident, and 80 days are required to clearly observe fibers (cf. Figure 5b).

Although precise kinetic investigations were not performed, the appearance of anisotropic microstructures is noticeable depending on the molecular weight of the p*n*BA block. While **V-2k** assembles within 1−3 h, **V-8k** and **V-14k** require 2−16 days and **V-38k** needs 2−3 months for structure formation under comparable conditions (1 mg conjugate per mL). This is

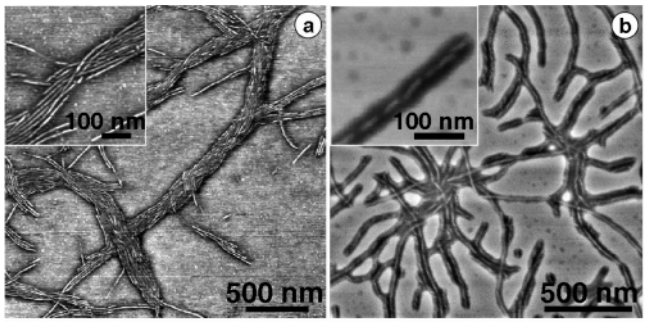

Figure 5. AFM micrographs of structures formed by the self-assembly of **IV-14k** (a) and **IV-38k** (b) in solution 16 and 80 days after inducing the switch process, respectively (Et_2O:MeOH = 70:30 vol %, c = 1 mg/mL; phase $z = 50°$ (a) and $z = 35°$ (b)).

expected because kinetics of assembly processes are strongly dependent on the volume faction of the peptide (ϕ^2). Hence, the apparent rates of the self-assembly of the conjugates decrease with increasing molecular weight of the p*n*BA block because molar concentration is reduced from 3.3×10^{-7} mol/mL (**V-2k**) to 2.5×10^{-8} mol/mL (**V-38k**). Moreover, secondary effects like the decrease of polymer end-group reactivity and accessibility should also be considered.

Despite the different rates of the self-assembly processes, all p*n*BA-*block*-$(TV)_5$ conjugates aggregate into fibrillar microstructures with dimensions in a rather comparable range. As it

could be anticipated the cross-sectional dimensions of the fiber aggregates increase consistently with the molecular weight of p*n*BA block from **V-8k** to **V-14k** to **V-38k** (Table 2). The strong analogy of the resulting structures to fibrils of β-sheet-forming peptides highlights that the organization of the peptide segment directs microstructure formation. For both high molecular weight analogs (**V-14k** and **V-38k**) this assumption could also be verified by spectroscopic and scattering techniques. FT-IR spectroscopy confirmed the presence of extended β-sheets, and SAED correlates the TEM images of the fibers with the β-sheet organization motif by showing a typical *d* spacing of 4.8 Å (Figure S6).

In analogy to the superhelices of **V-2k** and **V-8k** some evidence could be found suggesting the presence of a helical fine structure, even in the aggregates of **V-38k**. As shown in Figure 5b (inset) phase AFM imaging allows the visualization of periodic modulations along the fiber axis. Taking into account that the fibrillar structures of **V-14k** and **V-38k** exhibit (i) consistent dimensions to, e.g., the **V-8k** fibrils, (ii) extended β-sheet tapes, and (iii) evidence for a helical superstructure, it appears to be straightforward that an analogous aggregation model can be assumed. However, considering the amount of soft p*n*BA in **V-14k** (91.5 wt %) and **V-38k** (96.5 wt %) it is not surprising that a precise visualization of the distorted core−shell tapes in the assemblies is difficult.

It remains remarkable that with 8.5 and 3.5 wt % peptide content of **V-14k** and **V-38k**, respectively, the peptide segment still dominates and directs the structure formation process in the system. In these conjugates the peptide can be clearly considered as a functional polymer end group, which highlights the enormous potential of the class of monomer sequence-defined oligopeptides.

Conclusions

The synthesis and self-assembly behavior of a set of peptide−polymer conjugates was described. Conjugates were synthesized possessing poly(*n*-butyl acrylate) blocks (p*n*BA) with different block lengths but the same (threonine−valine)$_5$ peptide segment as a β-sheet-forming aggregator domain. The high aggregation tendency of the peptide segment was temporarily suppressed by both switch and pseudoproline defects, allowing an ease of synthesis and handling. To access conjugates with well-defined p*n*BA blocks (M_n = 8000−38 000 and M_w/M_n = 1.2−1.3) the RAFT polymerization approach was applied. The temporarily disturbed peptide segment was functionalized with a RAFT chain-transfer moiety, and the resulting peptide-CTA could effectively mediate the polymerization of *n*-butyl acrylate in solution. However, the native, undisturbed peptide segment was reestablished via a pH-controlled rearrangement in the defects, leading to conjugates with induced aggregation tendency and thus triggering the self-assembly process of the peptide−polymer conjugates. The peptide-directed microstructure formation was studied in organic solvents by slowly inducing the aggregation tendency. Atomic force microscopy (AFM) allowed visualization of fibrillar microstructures and provides evidence for a left-handed superhelical fine structure. The organization of the peptides in extended β-sheets is proven by infrared spectroscopy (FT-IR) and electron diffraction coupled to transmission electron microscopy (SAED-TEM). The dimensions of the fibrillar structures and approximated rates of microstructure formation are correlated to the molecular weights of the p*n*BA block in the conjugates. Thus, peptide organization was recognized to control the microstructure formation of a p*n*BA block ($M_n \approx$ 38 000) even at an oligopeptide organizer content of only 3.5 wt %.

Acknowledgment. Jessica Brandt, Katharina Ostwald, Arne Thomas, Anne Heilig, Marlies Gräwert, and, in particular, Andrea Grafmüller as well as Andreas Richter are thanked for their contributions to this project. We also thank Markus Antonietti for his continuous support and inspiring discussions. Financial support was received from the German Research Foundation through the Emmy Noether-Program (BO 1762/2-2) and the Max Planck Society.

Supporting Information Available: Materials, methods, and synthesis procedures for the switch-peptide precursor **I** and the switch-peptide chain-transfer agent (**II** and **III**) as well as molecular weight vs conversion plot of the RAFT polymerization of *n*BA mediated by **III**; characterization of the aggregation behavior of **IV-8k**, **IV-14k**, and **IV-38k** (FT-IR spectra, TEM images including SAED, and AFM micrographs). This material is available free of charge via the Internet at http://pubs.acs.org.

References and Notes

(1) Stryer, L. *Biochemistry*, 4th ed.; W. H. Freeman and Company: New York, 1995; p 1064.
(2) Creighton, T. E. *Protein Function: a Practical Approach*, 2nd ed.; Oxford University Press: New York, 1997; p 360.
(3) Whitford, D. *Proteins: Structure and Function*; Wiley & Sons: New York, 2005; p 542.
(4) Dwek, R. A. *Chem. Rev.* **1996**, *96*, 683.
(5) Whitesides, G. M. *Small* **2005**, *1*, 172.
(6) Börner, H. G.; Schlaad, H. *Soft Matter* **2007**, *3*, 394.
(7) Klok, H.-A. *J. Polym. Sci., Part A: Polym. Chem.* **2005**, *43*, 1.
(8) Klok, H.-A.; Schlaad, H. Peptide Hybrid Polymers. In *Advances in Polymer Science*; Springer: Berlin-Heidelberg, 2006; Vol. 202, p 160.
(9) Heredia, K. L.; Bontempo, D.; Ly, T.; Byers, J. T.; Halstenberg, S.; Maynard, H. D. *J. Am. Chem. Soc.* **2005**, *127*, 16955.
(10) Alemdaroglu, F. E.; Safak, M.; Wang, J.; Berger, R.; Herrmann, A. *Chem. Commun.* **2007**, 1358.
(11) Smeenk, J. M.; Otten, M. B. J.; Thies, J.; Tirrell, D. A.; Stunnenberg, H. G.; van Hest, J. C. M. *Angew. Chem., Int. Ed.* **2005**, *44*, 1968.
(12) Jahnke, E.; Lieberwirth, I.; Severin, N.; Rabe, J. P.; Frauenrath, H. *Angew. Chem., Int. Ed.* **2006**, *45*, 5383.
(13) Becker, M. L.; Liu, J.; Wooley, K. L. *Biomacromolecules* **2005**, *6*, 220.
(14) Akiyoshi, K.; Kohara, M.; Ito, K.; Kitamura, S.; Sunamoto, J. *Macromol. Rapid. Commun.* **1999**, *20*, 112.
(15) Tirrell, M.; Kokkoli, E.; Biesalski, M. *Surf. Sci.* **2002**, *500*, 61.
(16) Langer, R.; Tirrell, D. A. *Nature* **2004**, *428*, 487.
(17) Di Zio, K.; Tirrell, D. A. *Macromolecules* **2003**, *36*, 1553.
(18) Sun, X.-Y.; Shankar, R.; Börner, H. G.; Ghosh, T. K.; Spontak, R. J. *Adv. Mater.* **2007**, *19*, 87.
(19) Oroudjev, E.; Soares, J.; Arcdiacono, S.; Thompson, J. B.; Fossey, S. A.; Hansma, H. G. *Proc. Natl. Acad. Sci. U.S.A.* **2002**, *99*, 6460.
(20) Law, R.; Carl, P.; Harper, S.; Dalhaimer, P.; Speicher, D. W.; Discher, D. E. *Biophys. J.* **2003**, *84*, 533.
(21) Smith, B. L.; Schaffer, T. E.; Viani, M.; Thompson, J. B.; Frederick, N. A.; Kindt, J.; Belcher, A.; Stucky, G. D.; Morse, D. E.; Hansma, P. K. *Nature* **1999**, *399*, 761.
(22) Thompson, J. B.; Kindt, J. H.; Drake, B.; Hansma, H. G.; Morse, D. E.; Hansma, P. K. *Nature* **2001**, *414*, 773.
(23) Kellermayer, M. S. Z.; Smith, S. B.; Granzier, H. L.; Bustamante, C. *Science* **1997**, *276*, 1112.
(24) Guan, Z. *Polym. Int.* **2007**, *56*, 467.
(25) Fricke, M.; Schaedler, V. *Macromol. Biosci.* **2007**, *7*, 103. Complete issue: *Bioinspired Mater.* 93−240.
(26) Börner, H. G. *Macromol. Chem. Phys.* **2007**, *208*, 124.
(27) Lashuel, H. A.; LaBrenz, S. R.; Woo, L.; Serpell, L. C.; Kelly, J. W. *J. Am. Chem. Soc.* **2000**, *122*, 5262.
(28) Aggeli, A.; Bell, M.; Carrick, L. M.; Fishwick, C. W. G.; Harding, R.; Mawer, P. J.; Radford, S. E.; Strong, A. E.; Boden, N. *J. Am. Chem. Soc.* **2003**, *125*, 9619.
(29) Eckhardt, D.; Groenewolt, M.; Krause, E.; Börner, H. G. *Chem. Commun.* **2005**, 2814.
(30) Hentschel, J.; Krause, E.; Börner, H. G. *J. Am. Chem. Soc.* **2006**, *128*, 7722.
(31) Aggeli, A.; Nyrkova, I. A.; Bell, M.; Harding, R.; Carrick, L.; McLeish, T. C. B.; Semenov, A. N.; Boden, N. *Proc. Natl. Acad. Sci. U.S.A.* **2001**, *98*, 11857.
(32) Lutz, J.-F.; Börner, H. G. *Prog. Polym. Sci.* **2007**, http://dx.doi.org/10.1016/j.progpolymsci.2007.07.045.

(33) Roberts, M. J.; Bentley, M. D.; Harris, J. M. *Adv. Drug Deliv. Rev.* **2002**, *54*, 459.
(34) ten Cate, M. G. J.; Severin, N.; Börner, H. G. *Macromolecules* **2006**, *39*, 7831.
(35) Lutz, J.-F.; Börner, H. G.; Weichenhan, K. *Macromolecules* **2006**, *39*, 6376.
(36) Vandermeulen, G. W. M.; Tziatzios, C.; Klok, H. A. *Macromolecules* **2003**, *36*, 4107.
(37) Hellermann, H.; Lucas, H. W.; Maul, J.; Pillai, V. N. R.; Mutter, M. *Makromol. Chem.* **1983**, *184*, 2603.
(38) Braunecker, W. A.; Matyjaszewski, K. *Prog. Polym. Sci.* **2007**, *32*, 93.
(39) Becker, M. L.; Liu, J. Q.; Wooley, K. L. *Chem. Commun.* **2003**, 180.
(40) Rettig, H.; Krause, E.; Boerner, H. G. *Macromol. Rapid Commun.* **2004**, *25*, 1251.
(41) Mei, Y.; Beers, K. L.; Byrd, H. C. M.; Vanderhart, D. L.; Washburn, N. R. *J. Am. Chem. Soc.* **2004**, *126*, 3472.
(42) Ayres, L.; Hans, P.; Adams, J.; Lowik, D.; van Hest, J. C. M. *J. Polym. Sci., Part A: Polym Chem* **2005**, *43*, 6355.
(43) ten Cate, M. G. J.; Rettig, H.; Bernhardt, K.; Boerner, H. G. *Macromolecules* **2005**, *38*, 10643.
(44) Mutter, M.; Chandravarkar, A.; Boyat, C.; Lopez, J.; Dos Santos, S.; Mandal, B.; Mimna, R.; Murat, K.; Patiny, L.; Saucede, L.; Tuchscherer, G. *Angew. Chem., Int. Ed.* **2004**, *43*, 4172.
(45) Carpino, L. A.; Krause, E.; Sferdean, C. D.; Schuemann, M.; Fabian, H.; Bienert, M.; Beyermann, M. *Tetrahedron Lett.* **2004**, *45*, 7519.
(46) Sohma, Y.; Sasaki, M.; Hayashi, Y.; Kimura, T.; Kiso, Y. *Chem. Commun.* **2004**, 124.
(47) Coin, I.; Dolling, R.; Krause, E.; Bienert, M.; Beyermann, M.; Sferdean, C. D.; Carpino, L. A. *J. Org. Chem.* **2006**, *71*, 6171.
(48) Hentschel, J.; Börner, H. G. *J. Am. Chem. Soc.* **2006**, *128*, 14142.
(49) Janek, K.; Behlke, J.; Zipper, J.; Fabian, H.; Georgalis, Y.; Beyermann, M.; Bienert, M.; Krause, E. *Biochemistry* **1999**, *38*, 8246.
(50) Altmann, K. H.; Florsheimer, A.; Mutter, M. *Int. J. Pept. Protein Res.* **1986**, *27*, 314.
(51) Quibbel, M.; Johnson, T. *Difficult peptides. Fmoc Solid Phase Peptide Synthesis. A Practical Approach;* Oxford University Press UK: Oxford, 2000; pp 115−136.
(52) Wohr, T.; Wahl, F.; Nefzi, A.; Rohwedder, B.; Sato, T.; Sun, X. C.; Mutter, M. *J. Am. Chem. Soc.* **1996**, *118*, 9218.
(53) Boerner, H. G.; Beers, K.; Matyjaszewski, K.; Sheiko, S. S.; Moeller, M. *Macromolecules* **2001**, *34*, 4375.

MA071810Z